J. Fluid Mech. (2004), *vol.* 511, *pp.* 125–134. © 2004 Cambridge University Press
DOI: 10.1017/S0022112004009863 Printed in the United Kingdom

Internal wave tunnelling

By BRUCE R. SUTHERLAND AND KERIANNE YEWCHUK

Department of Mathematical and Statistical Sciences, University of Alberta, Edmonton, AB, Canada T6G 2G1

(Received 5 May 2004)

We present the first laboratory evidence of internal gravity wave tunnelling through weakly stratified fluid patches and we derive analytic theories for energy transmission by the waves in two distinct circumstances. In one, the computed transmission coefficient is directly analogous to the textbook calculation for quantum tunnelling of a free electron incident upon a potential barrier. In the other, we consider the partial reflection and transmission of internal waves through a mixed region bounded by discontinuities in the density profile. The results reveal a linear resonance between vertically propagating internal waves and interfacial waves that exist on either flank of the mixing region. The resonance permits perfect transmission of internal waves that would otherwise strongly reflect from the weakly stratified region. We discuss a specific application of our results to deep convective storm-generated internal waves that tunnel through the mesosphere to the ionosphere.

1. Introduction

Internal gravity waves propagate through a fluid whose density, $\bar{\rho}(z)$, decreases with height†, their motion being governed by buoyancy restoring forces. The maximum allowed frequency of propagating internal waves is the buoyancy frequency, N. In the Boussinesq approximation, in which density variations are important only as they affect buoyancy forces, the squared buoyancy frequency is proportional to the background density gradient: $N^2 = -(g/\rho_0)\mathrm{d}\bar{\rho}/\mathrm{d}z$, in which the g is the acceleration due to gravity and ρ_0 is a characteristic density of the fluid.

Internal waves vertically transport energy and momentum and so accelerate and mix the ambient fluid at levels where they break. Consequently they are known to affect significantly the mean circulations of the atmosphere (Palmer Shutts & Swinbank 1986; McFarlane 1987) and ocean (Polzin *et al.* 1997; Ledwell *et al.* 2000).

To determine where energy and momentum are transported and deposited it is typical to rely on the results of 'ray theory' (Lighthill 1978; Broutman *et al.* 1997; Hines 2002), which predicts the path followed by small-amplitude internal waves in a slowly varying background density and velocity field. In particular this methodology predicts that waves asymptotically approach a 'critical level', being the height where the horizontal phase speed of the waves matches the background flow speed. In stationary fluid the theory also predicts that the waves reflect from a level where the wave frequency matches the background buoyancy frequency N. It is the latter case that is of interest here.

† In the atmosphere, thermodynamic considerations require that the potential temperature increase with height, but in the Boussinesq approximation the dynamics of internal wave motions are effectively the same.

https://doi.org/10.1017/S0022112004009863 Published online by Cambridge University Press

Consider the upward propagation of an internal wavepacket in fluid that is uniformly stratified (constant N) below some level, z_r, and uniform density ($N = 0$) above. Ray theory predicts that the wavepacket would reflect from this level, although a closer examination of the problem reveals that the disturbance amplitude is not identically zero above z_r: the waves are evanescent and so the amplitude decreases exponentially with height above z_r. If a short distance above z_r the fluid becomes stratified once more, then we expect the wavepacket will partially transmit across and reflect from this uniform-density region. This is the process of internal gravity wave tunnelling.

Internal wave tunnelling between two regions of locally enhanced stratification (ducts) has previously been described theoretically by considering resonances between different vertical modes of the system. This was done by Eckart (1961) who considered energy transfers between internal wave modes of the main and seasonal thermocline in the ocean. Resonant transfers between ducts in the stratosphere and ionosphere were similarly described by Jones (1970) and Fritts & Yuan (1989), the latter additionally considering the effects of ducting by Doppler-shifting winds.

When resonances between ducted modes occur energy is transferred from one mode, whose amplitude is largest within one duct, to another mode whose amplitude is largest within the other duct. The tunnelling is an oscillatory process so that energy periodically transfers back and forth between the two ducts via this process.

Resonant mode theory is usefully applied to circumstances in which the vertical scale of the internal waves is comparable with the vertical scale of each duct – that is, for low-order modes. However, it cannot describe the irreversible one-way transfer of energy of small vertical-scale internal waves from one duct to another.

Independent of numerical simulations it would be convenient to estimate what fraction of energy transported by waves incident upon the mesosphere is transmitted through to the ionosphere. This paper provides the tools for making such an estimate.

More generally, this paper provides an analytic prediction for the transmission coefficient of internal waves crossing a region in which N^2 is reduced. This is done in two cases. In § 2, we consider wave propagation through a background characterized by a continuous, piecewise linear background density profile and through an idealized background density profile resulting from partial local mixing of an initially uniformly stratified fluid. The latter case is piecewise linear but exhibits discontinuous density jumps on either flank of the mixed region. Applications to laboratory experiments and to geophysical circumstances are discussed in § 3 and conclusions are given in § 4.

2. Theory

Assuming a stationary two-dimensional, Boussinesq fluid, small-amplitude waves are known to satisfy the following equation for the streamfunction ψ:

$$\left(\frac{\partial^2}{\partial x^2} + \frac{\partial^2}{\partial z^2}\right)\frac{\partial^2 \psi}{\partial t^2} + N^2 \frac{\partial^2 \psi}{\partial x^2} = 0. \tag{2.1}$$

We consider horizontally and temporally periodic solutions in two circumstances distinguished by the structure of N^2.

2.1. *Transmission across an N^2-barrier*

In this first case we prescribe

$$N^2 = \begin{cases} N_0^2, & |z| > L/2 \\ 0, & |z| \leqslant L/2. \end{cases}$$

https://doi.org/10.1017/S0022112004009863 Published online by Cambridge University Press

We call this an 'N^2-barrier' of depth L because, as we discuss in the Appendix, this circumstance is directly analogous to the quantum mechanical case in which a free electron tunnels across a potential barrier.

Solutions are a superposition of waves of the form $\psi = \hat{\psi}(z)\exp[\mathrm{i}(kx - \omega t)]$, in which the horizontal wavenumber, k, and frequency, $\omega\,(\leqslant N_0)$, are prescribed constants, and $\hat{\psi}$ is given by

$$\hat{\psi} = \begin{cases} A_3 \mathrm{e}^{\mathrm{i}\gamma z}, & z > L/2 \\ A_2 \mathrm{e}^{z/\delta} + B_2 \mathrm{e}^{-z/\delta}, & -L/2 < z < L/2 \\ A_1 \mathrm{e}^{\mathrm{i}\gamma z} + B_1 \mathrm{e}^{-\mathrm{i}\gamma z}, & z < -L/2, \end{cases} \tag{2.2}$$

with $\delta = 1/k$ and $\gamma = -k(N_0{}^2/\omega^2 - 1)^{1/2}$. Because γ represents the vertical wavenumber for $|z| > L/2$, it is defined to be negative so that incident waves (with amplitude A_1) and transmitted waves (with amplitude A_3) propagate upward.

Boundary conditions at $z = \pm L/2$ are given by requiring that the vertical velocity and pressure is continuous (Drazin & Reid 1981). For a fluid with zero mean flow this amounts to requiring that $\hat{\psi}(z)$ is continuous and differentiable. Thus the transmission coefficient, which represents the fraction of incident energy transported across the N^2-barrier, is given by

$$T = \left[1 + \frac{(\gamma^2\delta^2 + 1)^2}{(2\gamma\delta)^2}\sinh^2(L/\delta)\right]^{-1}. \tag{2.3}$$

We define $\Theta = \arccos(\omega/N_0)$, which represents the angle at which lines of constant phase are oriented from the vertical when $\omega \leqslant N_0$. Thus (2.3) becomes

$$T = \left[1 + \left(\frac{\sinh(kL)}{\sin 2\Theta}\right)^2\right]^{-1}. \tag{2.4}$$

In formulating (2.2) we have supposed that internal waves are incident from below the mixed region. Alternatively, we could allow the internal waves to be incident from above but the prediction (2.4) would not change because we are working in the Boussinesq approximation.

It is straightforward to generalize our result to the case of an N^2-barrier in which

$$N^2 = \begin{cases} N_0^2, & |z| > L/2 \\ N_1^2, & |z| \leqslant L/2. \end{cases}$$

For $N_1 \leqslant \omega \leqslant N_0$ ($\Delta^2 \geqslant 0$), the transmission coefficient is

$$T_{\mathrm{barrier}} = \left[1 + \left(\frac{1 - \sigma^2}{\Delta}\frac{\sinh(\kappa)}{\sin 2\Theta}\right)^2\right]^{-1}, \tag{2.5}$$

and for $\omega \leqslant N_1$

$$T_{\mathrm{barrier}} = \left[1 + \left(\frac{1 - \sigma^2}{\tilde{\Delta}}\frac{\sin(\tilde{\kappa})}{\sin 2\Theta}\right)^2\right]^{-1}. \tag{2.6}$$

In these formulae we have defined $\sigma^2 = N_1^2/N_0^2$, $\Delta^2 = 1 - \sigma^2\sec^2\Theta$, $\tilde{\Delta}^2 = -\Delta^2$, $\kappa = kL\Delta$ and $\tilde{\kappa} = kL\tilde{\Delta}$. Note that (2.6) holds even in the case $N_1^2 \geqslant N_0^2$. In particular, $T_{\mathrm{barrier}} = 1$ when $N_1^2 = N_0^2$, as expected.

Figure 1 plots values of the transmission coefficient as a function of kL and Θ for three cases, each with different values of σ^2. Figure 1(*a*), which corresponds to the

https://doi.org/10.1017/S0022112004009863 Published online by Cambridge University Press

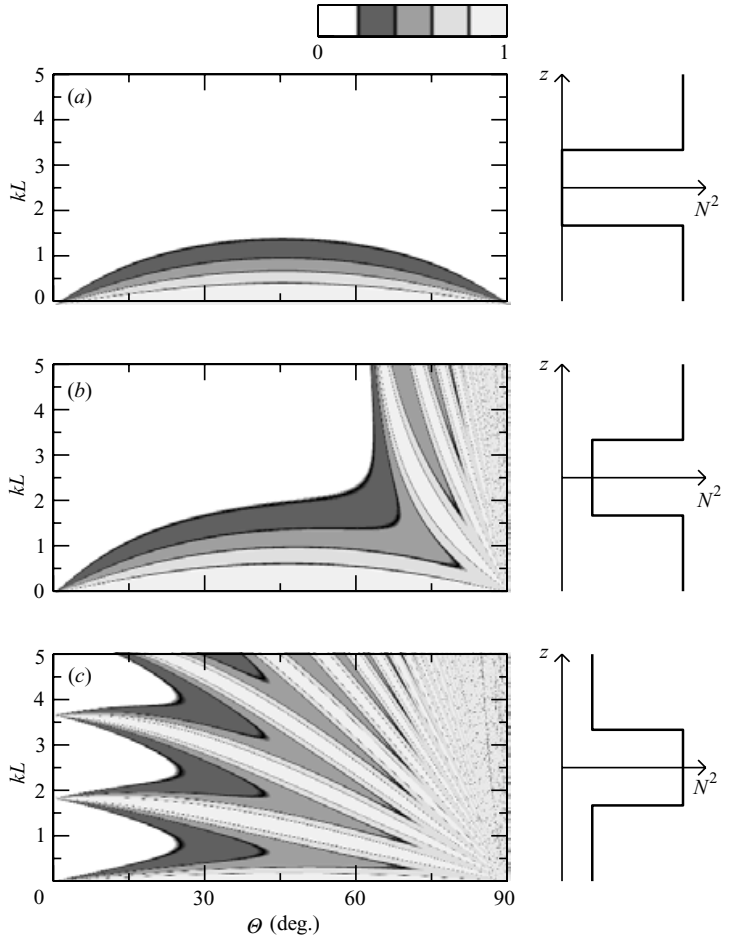


FIGURE 1. The colour contour plots to the left show values of the transmission coefficient, T_{barrier}, for internal gravity waves traversing an N^2-barrier with (*a*) $\sigma^2 = 0$, (*b*) $\sigma^2 = 1/4$ and (*c*) $\sigma^2 = 4$. $\Theta = \arccos(\omega/N_0)$ represents the angle of propagation of the incident waves with respect to the vertical. Schematics of the corresponding background N^2 profiles are shown to the right.

case with $N_1^2 = 0$, shows that transmission is greatly inhibited when the barrier width is larger than k^{-1}, or about a sixth of the horizontal wavelength, λ. Surprisingly, waves that propagate with frequency infinitesimally close to the buoyancy frequency (hence with $\Theta \gtrsim 0$) reflect from barriers of infinitesimally small width.

The case with $N_1^2 = N_0^2/4$ is shown in figure 1(*b*). Here, the waves are evanescent across the barrier if $\Theta < \cos^{-1}(\sqrt{\sigma}) = 60^\circ$. Waves with $\Theta > 60^\circ$ transmit with greater efficiency across the barrier for a discrete range of barrier widths corresponding to propagating waves coupling with trapped internal wave modes within the barrier. However, for these non-evanescent waves transmission is not always 100%.

In the case with $N_1^2 = 4N_0^2$ (figure 1*c*) resonant modes exist for all values of Θ. For $\Theta = 0$, resonance peaks occur if $kL = n\pi/(\sigma^2 - 1)^{1/2} = n\pi/3^{1/2}$, for positive integers, n. However, particularly for small Θ, transmission is small for a broad range of kL even though $\omega < N(z)$ everywhere. Inappropriately applying ray theory to this circumstance would yield the misleading prediction that 100% transmission occurs for all kL and Θ.

https://doi.org/10.1017/S0022112004009863 Published online by Cambridge University Press

2.2. *Transmission across a locally mixed region*

In the circumstance considered above, $\overline{\rho}(z)$ is assumed to vary continuously, even though its slope is discontinuous at $z = \pm L/2$. More realistically, localized mixed regions within a stratified fluid are better represented by a discontinuous density profile generically of the form

$$\overline{\rho} = \begin{cases} \rho_0(1 - z/H_1), & |z| \leqslant L/2 \\ \rho_0(1 - z/H_0), & |z| > L/2, \end{cases} \tag{2.7}$$

in which $H_0 \equiv g/N_0^2$ and $H_1 \equiv g/N_1^2$ measure the strength of stratification respectively outside and within a partially mixed region of depth L. Consistent with the Boussinesq approximation, we assume $H_0, H_1 \gg L, k^{-1}$. The corresponding squared buoyancy frequency (a 'mixed-N^2' profile) is the same as that for the generalization of the 'N^2-barrier' except for infinite spikes at $z = \pm L/2$ where the density changes discontinuously by $\Delta\rho = \rho_0[(N_0^2 - N_1^2)/g](L/2)$.

To compute the transmission coefficient in the case $N_1 \leqslant \omega \leqslant N_0$, we find that $\hat{\psi}$ is given by (2.2) with $\gamma = -k(N_0^2/\omega^2 - 1)^{1/2}$ and $\delta^{-1} = k(1 - N_1^2/\omega^2)^{1/2}$. Requiring the vertical velocity to be continuous at $z = \pm L/2$ imposes the restriction that $\hat{\psi}$ is continuous. However, the condition for continuous pressure requires that the combination $\overline{\rho}(\hat{\psi}' - \hat{\psi}\, gk^2/\omega^2)$ is continuous (Drazin & Reid 1981).

Proceeding as before (though with considerably more algebra), the transmission coefficient is

$$T_{\text{mix}} = \left[1 + \left(\frac{1 - \sigma^2}{\Delta}\frac{\sinh(\kappa)}{\sin 2\Theta}\Gamma\right)^2\right]^{-1}, \tag{2.8}$$

in which

$$\Gamma = 1 + \frac{1}{4}\frac{\kappa^2}{\cos^2\Theta}\frac{1 - \sigma^2}{\Delta^2} - \kappa\coth(\kappa). \tag{2.9}$$

In the case $\omega < N_1$, the transmission coefficient is

$$T_{\text{mix}} = \left[1 + \left(\frac{1 - \sigma^2}{\tilde{\Delta}}\frac{\sin(\tilde{\kappa})}{\sin 2\Theta}\tilde{\Gamma}\right)^2\right]^{-1}, \tag{2.10}$$

in which

$$\tilde{\Gamma} = 1 + \frac{1}{4}\frac{\tilde{\kappa}^2}{\cos^2\Theta}\frac{1 - \sigma^2}{\tilde{\Delta}^2} - \tilde{\kappa}\cot(\tilde{\kappa}). \tag{2.11}$$

Contours of these transmission coefficients are shown in figure 2 for the case with (*a*) $N_1^2 = 0$ and (*b*) $N_1^2 = N_0^2/4$. (Study of the case $N_1^2 = 4N_0^2$ is meaningless here.)

An obvious difference between the N^2-barrier and this mixed-N^2 case is that internal gravity waves generally transmit more effectively through the region where N^2 is reduced. For example, consider waves propagating with the fastest vertical group velocity (i.e. with $\Theta = \arccos((2/3)^{1/2}) \simeq 35°$) and with horizontal wavelength one quarter the width of the reduced N^2 region (i.e. with $kL = \pi/2$). In the case $\sigma = 0$, internal gravity waves transport 79% of incident energy across a mixed-N^2 region but transport only 14% across an N^2-barrier.

A second notable feature of the predicted transmission coefficient is the transmission spike for waves with small Θ and $kL \simeq 2.4$. This occurs due to a linear coupling between interfacial waves at $z = \pm L/2$ and propagating internal gravity waves outside

https://doi.org/10.1017/S0022112004009863 Published online by Cambridge University Press

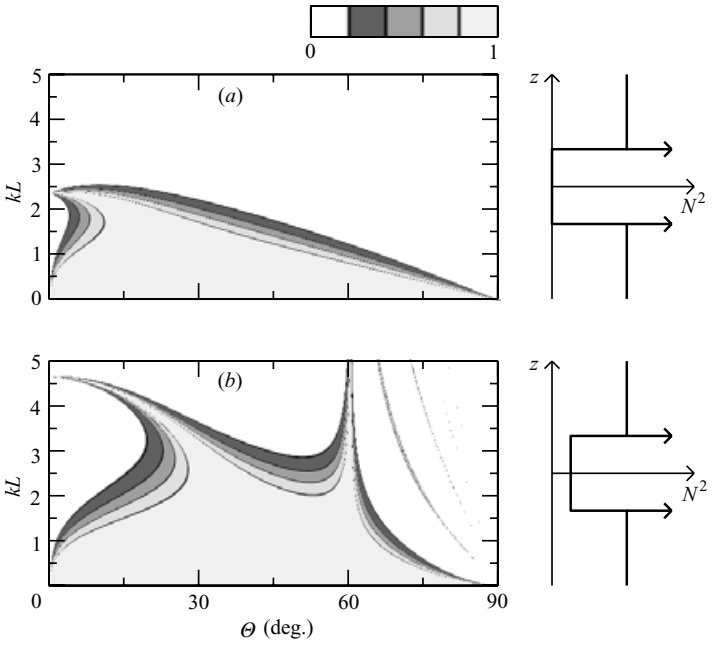


FIGURE 2. As in figure 1(*a*,*b*) but showing values of the transmission coefficient, T_{mix}, for internal gravity waves traversing a mixed-N^2 region with (*a*) $\sigma^2 = 0$ and (*b*) $\sigma^2 = 0.25$. The rightward-pointing arrows drawn on the N^2 profiles indicate where jump discontinuities occur in the corresponding background density profiles.

the mixed region. The dispersion relation for an interfacial wave in a two-layer fluid is $\omega^2 = g(\Delta\rho/\rho_0)k$. For a sufficiently wide mixed region, and assuming that the stratification outside this region has a relatively small effect on changing the frequency of the interfacial waves, we estimate $\omega \simeq N_0(kL/2)^{1/2}$. Away from the mixed region internal waves with $\Theta \simeq 0^\circ$ have frequency close to N_0. Matching the two frequency estimates gives $kL \simeq 2$, on the order of the observed value where the transmission spike occurs.

Like the N^2-barrier case, here additional transmission spikes occur in bands when $\omega < N_1$ (see figure 2*b*). However, these bands are considerably more narrow. Thus the presence of density interfaces acts more selectively to filter waves with vertical wavelengths that are short compared with their horizontal wavelengths.

3. Applications

3.1. *Laboratory experiments*

Internal wave tunnelling is immediately visualizable in laboratory experiments, the results of which are shown in figure 3. In these experiments a 197 cm long tank is filled 30 cm deep with uniformly salt-stratified water. A circular cylinder of radius $R = 2.1$ cm whose length spans the width of the tank is suspended with its centre approximately 6 cm below the surface and 24 cm above the bottom of the tank. By vertically oscillating the cylinder with frequency (here $0.5\,\mathrm{s}^{-1}$) moderately below the buoyancy frequency (here $N_0 = 1.1\,\mathrm{s}^{-1}$), the classic cross-pattern of waves is generated (Mowbray & Rarity 1967).

https://doi.org/10.1017/S0022112004009863 Published online by Cambridge University Press

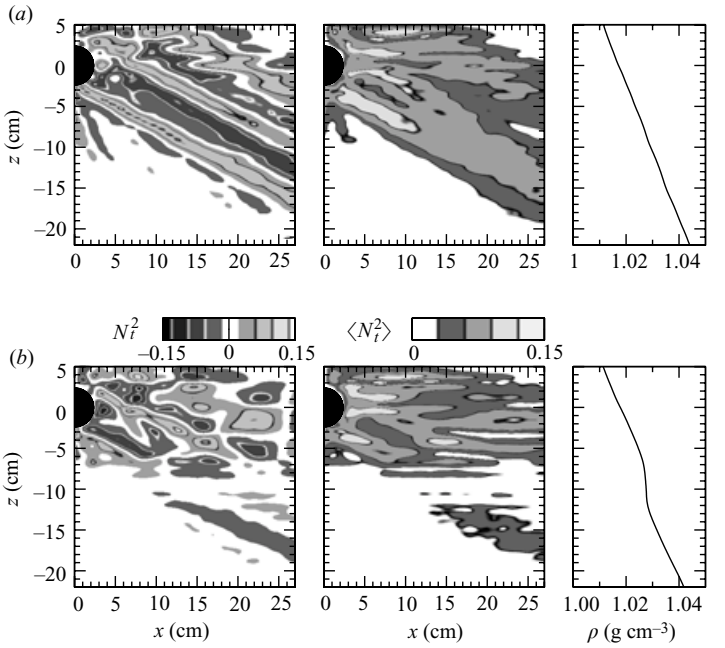


FIGURE 3. Internal wave beams generated in laboratory experiments by a vertically oscillating cylinder that (*a*) propagate downward and to the right in uniformly stratified fluid and (*b*) partially transmit across and reflect from an N^2-barrier. The left-hand panels show the instantaneous rate of change of the perturbation squared buoyancy frequency field, N_t^2, which is proportional to the time derivative of the horizontally averaged density gradient, $\partial\rho/\partial z$. The field is normalized by $N_0^3 A/R$, in which A and R are the oscillation amplitude and radius of the cylinder, respectively. Where $N(z) = N_0$, the field is proportional to the vertical displacement of fluid induced by the waves. The middle panels show the amplitude envelope of the same normalized field. The portion of the cylinder in the field-of-view drawn in black on the four contour plots. The right panels show the corresponding measured profiles of background density.

The contour plots in figure 3(*a*) focus upon one of the four wave beams, specifically the one that propagates downward to the right of the cylinder. The contours are determined using 'synthetic schlieren' (Sutherland *et al.* 1999; Sutherland & Linden 2002). This non-intrusive technique visualizes and measures internal wave amplitudes by determining changes to the squared buoyancy frequency resulting from the stretching and compression of isopycnal surfaces due to waves. The amplitude envelope clearly shows a primary downward beam whose centreline emanates from the cylinder, centred at $(x, z) = (0, 0)$, to approximately $(27, -15)$. The slope of the primary beam is determined by the ratio of the cylinder's oscillation frequency to the buoyancy frequency. To the immediate right of the cylinder, the disturbance field is complicated by waves that propagate upward from the cylinder and reflect from the surface at $z = 6$ cm. However, their presence is inconsequential for this study. Waves reflect from the lower boundary outside the field of view.

In a second experiment, the density profile is modified to be close to that of an N^2-barrier. This is done by putting a gate near one end of the tank, mixing the fluid behind it and then extracting the gate. The resulting intrusive gravity current and return flow ultimately establish a region of low N^2 at mid-depth and moderately

https://doi.org/10.1017/S0022112004009863 Published online by Cambridge University Press

enhanced stratification above and below. The depth of the mixed region is set either by repeatedly releasing intrusions or by inserting the gate farther from the tank end.

Figure 3(*b*) shows waves generated from an oscillating cylinder as in the first experiment, but here the waves propagate in non-uniformly stratified fluid. The measured density profile, plotted in the rightmost panel, crudely corresponds to an N^2-barrier of depth $L \simeq 3\,\mathrm{cm}$ and with $N_0 = 1.1\,\mathrm{s}^{-1}$ and $N_1 = 0$. The contour plots clearly show waves propagating below the mixed region: the waves have effectively tunnelled through a barrier.

The leftmost panel shows that the phase of the waves shifts above and below the barrier. This results from the wave being evanescent as it passes through the mixed region. Though the streamfunction field would show an exponential decrease in amplitude, the N_t^2 field shows vanishing waves near $z = -10\,\mathrm{cm}$. This is because the amplitude of the N_t^2 field is proportional to the cube of the background buoyancy frequency, which at that level is approximately zero.

The amplitude envelopes of the waves in the two experiments can be used to compute the transmission coefficient. Taking the ratio of the squared amplitude of the beam below the mixed region in the second experiment and the beam in the first experiment gives $T \simeq 0.5$. Crudely comparing this with theory, we take $\Theta \simeq 63^\circ$ and $k \simeq 2\pi/(4R/\cos\Theta) \simeq 0.34\,\mathrm{cm}^{-1}$. Thus equation (2.4) predicts $T_{\mathrm{barrier}} \simeq 0.3$. Despite the crude estimates of k and L, this value is close to the experimentally determined transmission coefficient.

To compare theory with experiments more accurately we would also need to account for dispersion and dissipative effects. A still more accurate theoretical comparison would use the measured profile of the background buoyancy frequency rather than an approximate piecewise-linear profile. Such calculations are beyond the scope of this paper.

3.2. *Geophysical applications*

In the experimental circumstance just considered, a quick calculation produced a reasonable estimate of the fraction of energy transmitted by internal waves across a region of reduced buoyancy frequency. Another example arises from recent atmospheric research.

Short-period internal waves generated by deep tropical convection have been observed to reach the ionosphere where they are visualized by OH airglow (Yamada *et al.* 2001). Simulations by Walterscheid, Schubert & Brinkman (2001)) show that wavepackets originating from the storm can tunnel through an evanescent region in the mesosphere to reach the ionosphere, where they evolve to become ducted modes. Alternative simulations by Snively & Pasko (2003) considered the propagation of longer-period non-evanescent waves through the mesosphere that consequently broke in the ionosphere.

In their simulations of internal wave tunnelling through the mesosphere to the lower thermospheric duct, Walterscheid *et al.* (2001) characterized the ducting as 'strong' or 'leaky' depending upon the wavelength and period of the incident waves. Assuming that the Boussinesq approximation captures the leading-order dynamics of the tunnelling waves, (2.5) provides a crude estimate of the leakiness.

From the N^2 profile given in figure 1 of Walterscheid *et al.* (2001), we characterize the squared buoyancy frequency within and outside the evanescent region by $N_1^2 \simeq 0.00025\,\mathrm{s}^{-2}$ and $N_0^2 \simeq 0.0005\,\mathrm{s}^{-2}$, respectively. For leaky incident waves with horizontal wavelength $2\pi/k \simeq 15\,\mathrm{km}$ and period $2\pi/\omega = 390\,\mathrm{s}$, the depth of the evanescent region determined from altitude profiles of m^2 is approximately $L = 5\,\mathrm{km}$. Thus we find the

https://doi.org/10.1017/S0022112004009863 Published online by Cambridge University Press

following non-dimensional variables: $\sigma^2 \simeq 0.5$, $\Theta \simeq 44°$, $\Delta^2 \simeq 0.037$ and $\kappa \simeq 0.40$. Using (2.5), the transmission coefficient is $T_{\text{barrier}} \simeq 0.5$, which indicates that approximately half the incident energy would be transported into the ionosphere. For strongly ducted incident waves with horizontal wavelength $2\pi/k \simeq 25\,\text{km}$ and period $2\pi/\omega = 309\,\text{s}$, the depth of the evanescent region is approximately $L = 30$ km. In this case $T_{\text{barrier}} \simeq 3 \times 10^{-4}$, a negligibly small value, as expected.

4. Conclusions

We have derived an analytic prediction for internal waves tunnelling through weakly stratified fluid and have provided experimental evidence of these dynamics. The main advance of the theory is that it provides, for the first time, quantitative predictions of the partial reflection and transmission of internal waves incident upon a weakly stratified layer. Thus one can now make *a priori* estimates of internal wave transmission in background profiles that vary vertically on scales smaller than or comparable with the scale of the waves, such as mesoscale ($O(10\,\text{km})$) waves in the atmosphere and small-scale ($O(10\,\text{m})$) waves in the ocean. Ray theory is inapplicable in such circumstances.

We are exploring a number of research paths leading from this work. In particular, we will extend these results to successively more complex and more realistic background profiles of N^2 and wind U, we will examine anelastic and finite-amplitude effects, and we will study specifically how internal waves generated near the ocean surface are filtered by multiple mixed patches (for example, due to salt-fingering) as they propagate downward into the deep ocean.

The authors are grateful to A. Kauffman for discussions regarding Eckart resonance. This research was supported by the Canadian Foundation for Climate and Atmospheric Science (CFCAS).

Appendix. Comparison with quantum mechanics

Schrödinger's equation is used to predict the transmission of a quantum 'particle' of mass m_0 and energy E_0 through a potential barrier of width L and maximum potential V_0. At the edges of the barrier the wavefunction must be continuously differentiable, just as required for the streamfunction in the N^2-barrier case. Thus the formula for the transmission coefficient is identical to (2.3) except that γ and δ are instead given by $\gamma = (2m_0E_0)^{1/2}/\hbar$ and $\delta = \mathrm{i}\hbar/(2m_0(E_0 - V_0))^{1/2}$.

Note that ray theory has the effect of treating waves like particles. Thus, just as classical theory incorrectly predicts electrons should entirely reflect from a potential barrier, so ray theory incorrectly predicts that internal waves should reflect entirely from well-mixed regions. The result is a reminder that ray theory is an approximation that fails when waves (quantum or classical) are of the same scale as the variations in the medium in which they propagate.

REFERENCES

Broutman, D., Macaskill, C., McIntyre, M. E. & Rottman, J. W. 1997 On Doppler-spreading models of internal waves. *Geophys. Res. Lett.* **24**, 2813–2816.

Drazin, P. G. & Reid, W. H. 1981 *Hydrodynamic Stability*. Cambridge University Press.

Eckart, C. 1961 Internal waves in the ocean. *Phys. Fluids* **4**, 791–799.

https://doi.org/10.1017/S0022112004009863 Published online by Cambridge University Press

Fritts, D. C. & Yuan, L. 1989 An analysis of gravity wave ducting in the atmosphere: Eckart's resonances in thermal and Doppler ducts. *J. Geophys. Res.* **94**(D15), 18455–18466.

Hines, C. O. 2002 Nonlinearities and linearities in internal gravity waves of the atmosphere and oceans. *Geophys. Astrophys. Fluid Dyn.* **96**, 1–30.

Jones, W. L. 1970 A theory for quasi-periodic oscillations observed in the ionosphere. *J. Atmos. Terres. Phys.* **32**, 1555–1566.

Ledwell, J. R., Montgomery, E., Polzin, K., St.Laurent, L. C., Schmitt, R. & Toole, J. 2000 Evidence for enhanced mixing over rough topography in the abyssal ocean. *Nature* **403**, 179–182.

Lighthill, M. J. 1978 *Waves in Fluids.* Cambridge University Press.

McFarlane, N. A. 1987 The effect of orographically excited gravity wave drag on the general circulation of the lower stratosphere and troposphere. *J. Atmos. Sci.* **44**, 1775–1800.

Mowbray, D. E. & Rarity, B. S. H. 1967 A theoretical and experimental investigation of the phase configuration of internal waves of small amplitude in a density stratified liquid. *J. Fluid Mech.* **28**, 1–16.

Palmer, T. N., Shutts, G. J. & Swinbank, R. 1986 Alleviation of a systematic westerly bias in general circulation and numerical weather prediction models through an orographic gravity drag parametrization. *Q. J. R. Met. Soc.* **112**, 1001–1039.

Polzin, K. L., Toole, J. M., Ledwell, J. R. & Schmitt, R. W. 1997 Spatial variability of turbulent mixing in the Abyssal Ocean. *Science* **276**, 93–96.

Snively, J. B. & Pasko, V. P. 2003 Breaking of thunderstorm-generated gravity waves as a source of short-period ducted waves at mesopause altitudes. *Geophys. Res. Lett.* **30**(24), 2254.

Sutherland, B. R., Dalziel, S. B., Hughes, G. O. & Linden, P. F. 1999 Visualisation and measurement of internal waves by "synthetic schlieren". Part 1: Vertically oscillating cylinder. *J. Fluid Mech.* **390**, 93–126.

Sutherland, B. R. & Linden, P. F. 2002 Internal wave excitation by a vertically oscillating elliptical cylinder. *Phys. Fluids* **14**, 721–731.

Walterscheid, R. L., Schubert, G. & Brinkman, D. G. 2001 Small-scale gravity waves in the upper mesosphere and lower thermosphere generated by deep tropical convection. *J. Geophys. Res.* **106**(D23), 31825–31832.

Yamada, Y., Fukunishi, H., Nakamura, T. & Tsuda, T. 2001 Breaking of small-scale gravity waves and transition to turbulence observed in OH airglow. *Geophys. Res. Lett.* **28**(11), 2153–2156.

https://doi.org/10.1017/S0022112004009863 Published online by Cambridge University Press